International Journal of Microwave and Wireless Technologies

cambridge.org/mrf

Introduction of the orthogonal mode via the polarization conversion parasitic structure for the isolation enhancement of MIMO patch antennas

Zhonghong Du[1], Xiaohui Zhang[1], Peiyu Qin[1,2], Yurong Pu[1] and Xiaoli Xi[1]

[1]The Faculty of Automation and Information Engineering, Xi'an University of Technology, Xi'an, China and
[2]Department of Electronic and Electrical Engineering, Brunel University London, London, UK

Research Paper

Cite this article: Du Z, Zhang X, Qin P, Pu Y, Xi X (2024) Introduction of the orthogonal mode via the polarization conversion parasitic structure for the isolation enhancement of MIMO patch antennas. *International Journal of Microwave and Wireless Technologies*, 1–9. https://doi.org/10.1017/S1759078724000461

Received: 12 July 2023
Revised: 15 March 2024
Accepted: 21 March 2024

Keywords:
isolation enhancement; MIMO antenna; polarization conversion; weak-field region construction

Corresponding author: Xiaohui Zhang;
Email: xhzhang@xaut.edu.cn

Abstract

In this study, a high-isolation multiple-input multiple-output (MIMO) microstrip patch antenna (MPA), which utilizes an orthogonal mode cancellation method is proposed. This method employs TM_{10} and TM_{01} modes, which are simultaneously excited in the rectangular passive MPA. Initially, a rectangular decoupling structure featuring polarization rotation characteristics is designed. Further studies show that by loading the polarization conversion parasitic structure (PCPS), the electric field of the spatial coupling wave can be transformed from the x-polarized TM_{10} mode to the y-polarized TM_{01} mode. Therefore, TM_{10} and TM_{01} modes from the excited antenna and decoupling structure are concurrently coupled to the passive antenna, forming an evident weak-field region on the passive antenna. Placing the feeding probe of the passive MPA within the weak-field region prevents signal reception at the port. Consequently, this results in an extremely low mutual coupling of −49 dB at a resonant frequency of 5.8 GHz. Finally, a prototype of the proposed antenna is fabricated and tested, and the measured results closely match the simulated results. Additionally, it is observed that PCPS slightly influences the performance of the MIMO antenna.

Introduction

Wireless local area networks (WLANs) play a pivotal role in connecting wireless devices. Their applications in the 5.8-GHz band have transformed connectivity by supporting more devices and facilitating higher transmission rates [1]. This is especially significant in the context of fifth- and sixth-generation mobile communications. Specifically, the use of multiple-input multiple-output (MIMO) antenna arrays plays a crucial role in enhancing transmission rates and channel capacity, achieving this without the need for additional spectrum resources or increased transmission power. However, this approach presents challenges in antenna design, especially when dealing with co-frequency and co-polarization antennas that are closely situated within the E- or H-plane. This scenario leads to strong mutual coupling between antenna elements, which in turn can cause issues such as impedance mismatch, distortion in the radiation pattern, and a decrease in realized gain [2, 3]. Therefore, enhancing isolation is a crucial aspect for designing WLAN-MIMO antennas [4–8].

Recently, several scholars proposed various decoupling methods to address the problem of strong mutual coupling between MIMO antenna elements. Based on the origin of the coupling waves, the techniques for minimizing coupling can be categorized into two main types: (i) direct suppression, which includes methods such as utilizing defected ground structures (DGSs) [9, 10], electromagnetic (EM) bandgap structures [11], and metasurfaces/metamaterials [12, 13]. These are employed to mitigate the coupling of floor currents, surface currents, and space waves, respectively; (ii) cancellation schemes, where the original coupling field is counteracted by a field produced through a decoupling structure. Common structures include the neutralization line [14], decoupling network [15, 16], polarization-conversion isolator [17–19], and parasitic elements [20, 21]. Additionally, recently received considerable attention, the self-decoupling method can be classified as a cancellation type. Distinguished from other traditional decoupling methods, the self-decoupling method makes use of the advantageous features of the antenna itself to reduce mutual coupling between MIMO antenna elements, without the necessity for additional decoupling structures [22–25]. For example, Lin et al. [22] engineered a microstrip patch antenna (MPA) using an inset-fed design. When the geometric parameters of the feeding structure are optimally configured, the fields generated by the feeding structure and radiation patch counteract each other. This creates a region of weak field on the ground plane. By positioning the antenna elements within this weak-field area of the adjacent elements, high isolation between MIMO antenna elements is realized, eliminating the need for a separate decoupling structure. A similar study, as reported in paper [23], involved the simultaneous excitation of TM_{10} and TM_{02} modes in a patch antenna. By fine-tuning the frequency of these two modes, the electric fields (E-fields) coupled to an unexcited patch antenna counteract each other, resulting in a distinct null-field region. As highlighted in prior research, while traditional decoupling schemes are effective in enhancing isolation to approximately 20 dB or more, they exhibit several drawbacks, such as increased physical profile [12, 13], complex antenna structure [17, 18], and compromised matching, and radiation performance. Simultaneously, the self-decoupling scheme, despite attracting significant research interest, presents its own challenges, for example, (i) the challenge in exciting or introducing the required mode and (ii) different arrangements of antenna elements and the method of weak-field generation leading to limitations in practical applications.

Furthermore, previous studies suggest that most decoupling methods are suitable for narrowband MIMO antennas. Therefore, the coupling suppression of broadband MIMO antennas has attracted the attention of numerous researchers [26–28]. In MPA, the methods commonly used to improve bandwidth include loading parasitic elements [26, 29], multimode technology [27, 30], and introducing metasurfaces [31]. Tran et al. [26] reported that by introducing parasitic elements, the bandwidth of an MIMO antenna was improved by approximately 4.8%, and the isolation was improved to more than 30 dB. Yuan et al. [27] proposed a planar inverted-F MIMO antenna that operates with a wide bandwidth of 78% using the multimode technology.

In general, in a rectangular MPA array, the field distributions of the excited antenna and coupled antenna element are in the TM_{10} mode. This study proposes a polarization conversion parasitic structure (PCPS), which can convert the x-polarized TM_{10} mode of the coupled E-field to the y-polarized TM_{01} mode. Consequently, the coupled fields of the two orthogonal modes cancel each other in the adjacent passive unexcited MPA, resulting in a specific weak-field region. The results show that when the feed probe of the unexcited MPA is intentionally placed in the weak-field region, the unexcited MPA cannot be excited effectively, and a low mutual coupling of approximately −49 dB can be obtained at 5.8 GHz. The effect of the decoupling structure on antenna performance is small and can thus be applied to multielement MIMO antenna arrays.

Design and analysis of polarization converter parasitic structure

In this section, the design and analysis of the proposed rectangular-ring PCPS are described. The structure of a PCPS is shown in Fig. 1(a). A rectangular metallic ring, tilted at 45° with respect to the x-axis, was mounted on top of an FR-4 substrate. This substrate exhibited a relative permittivity of 4.3 and a thickness of 1.6 mm. Below it, a metallic ground plane was established as the base layer. The simulation of this arrangement was conducted using CST Microwave Studio Software, setting up boundary conditions in the Floquet port. To determine the characteristics of an infinite periodic structure, its unit cells were simulated. The incident E-field was aligned with the z-axis. The parameters of the unit cell, set as $W_\mathrm{d} = 18$ mm, $L_\mathrm{r} = 10$ mm, and $W_\mathrm{r} = 5$ mm, were carefully selected to align the operating bandwidth of the proposed rectangular-ring PCPS with that of the antenna.

Consider the normal incident y-polarized EM wave as an example, denoted as E_y^i. The reflection coefficient and polarization conversion ratio (PCR) of the rectangular-ring PCPS are illustrated in Fig. 1(b). The reflected EM wave comprises co-polarized (r_{yy}) and cross-polarized (r_{xy}) reflections, defined as $r_{yy} = |\vec{E}_y^r| / |\vec{E}_y^i|$ and $r_{xy} = |\vec{E}_x^r| / |\vec{E}_x^i|$, respectively. Given that the rectangular ring is symmetrical in y- and x-directions, the simulated results of x-polarized incident EM waves are the same as those of y-polarized EM waves. Figure 1(b) illustrates that r_{yy} values are less than −10 dB while those of r_{xy} were approximately 0 dB in the range of 5.6–6.3 GHz. Furthermore, PCR indicates the polarization conversion efficiency, which can be expressed as follows [32]:

$$PCR = |r_{xy}|^2 / \left(|r_{yy}|^2 + |r_{xy}|^2 \right) \tag{1}$$

where r_{yy} and r_{xy} are obtained from Fig. 1(b). Meanwhile, effective polarization conversion is realized, as shown in Fig. 1(b), due to the PCR value, which is approximately 100% at 5.8 GHz.

To understand the operating principle of the rectangular metal ring, the induced current distributions of the rectangular ring element when the normal incident wave is y-polarized are shown in Fig. 2(a). The opposite induced current was excited on the rectangular metal ring and floor, indicating that the magnetic resonance was generated at 5.8 GHz. Furthermore, Fig. 2(b) shows that the induced magnetic field $\vec{H}^r$ along the lower right direction decomposes into two orthogonal components $\vec{H}_x^r$ and $\vec{H}_y^r$ along x- and y-axes, respectively. The component $\vec{H}_x^r$ is perpendicular to the incident E-field $\vec{E}_y^i$, with no cross-coupling between the induced magnetic field and induced E-field. Thus, component $\vec{H}_x^r$ does not contribute to the polarization conversion. Conversely, component $\vec{H}_y^r$ is parallel to the incident electric E-field $\vec{E}_y^i$, which induces an E-field perpendicular to $\vec{E}_y^i$. Consequently, the strong cross-coupling between the induced magnetic field and E-field is generated by $\vec{H}_y^r$, thereby, converting the incident wave from y-polarized to that of the reflection wave in x-polarized. Specifically, the magnetic field component parallel to the incident E-field causes the polarization conversion effect. The proposed rectangular ring can be regarded as a polarization converter in the desired operating bandwidth. Regarding the mechanism for reducing mutual coupling, the directional state of the coupling current is a critical factor in enhancing isolation between antenna elements. Consequently, the properties of PCPS can be leveraged to improve isolation due to their capability to alter the direction of the surface coupling current.

Design and analysis of two-element decoupling MPA

In this section, the configuration of a 1 × 2 MIMO MPA array is introduced first. Then, the decoupling mechanism is analyzed in detail.

Design and analysis of the proposed antenna

Figure 3 illustrates the two-element decoupled MIMO MPA structure constructed on an FR-4 substrate with a dielectric constant of 4.3 and an overall size of $41 \times 41 \times 1.6$ mm^3. Both MPAs were coaxially fed. The edge-to-edge and center-to-center distances between the two patches were $d = 12$ mm ($0.23\lambda_0$) and $d_1 = 22$ mm ($0.42\lambda_0$), respectively, where λ_0 denotes the wavelength in free space at a resonant frequency of 5.8 GHz. The proposed decoupling structure comprises three rectangular ring PCPSs arranged along the y-axis. According to the analysis described in the previous section, the decoupling structure can convert the polarization mode

https://doi.org/10.1017/S1759078724000461 Published online by Cambridge University Press

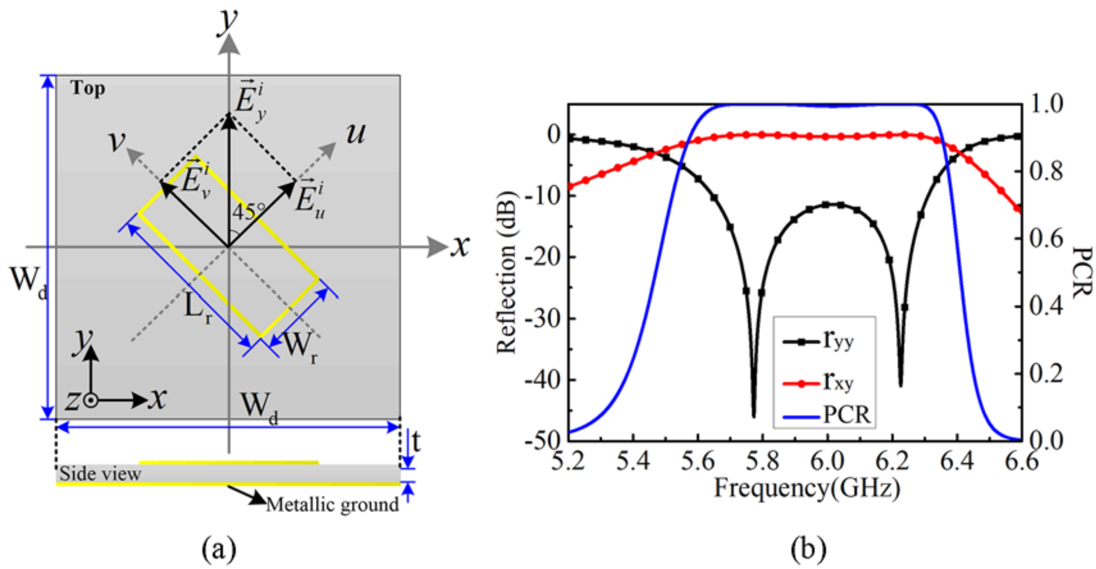

Figure 1. Structures and simulated results of rectangular ring PCPS. (a) Top and side view. (b) Co- and cross-polarization coefficients and PCR.

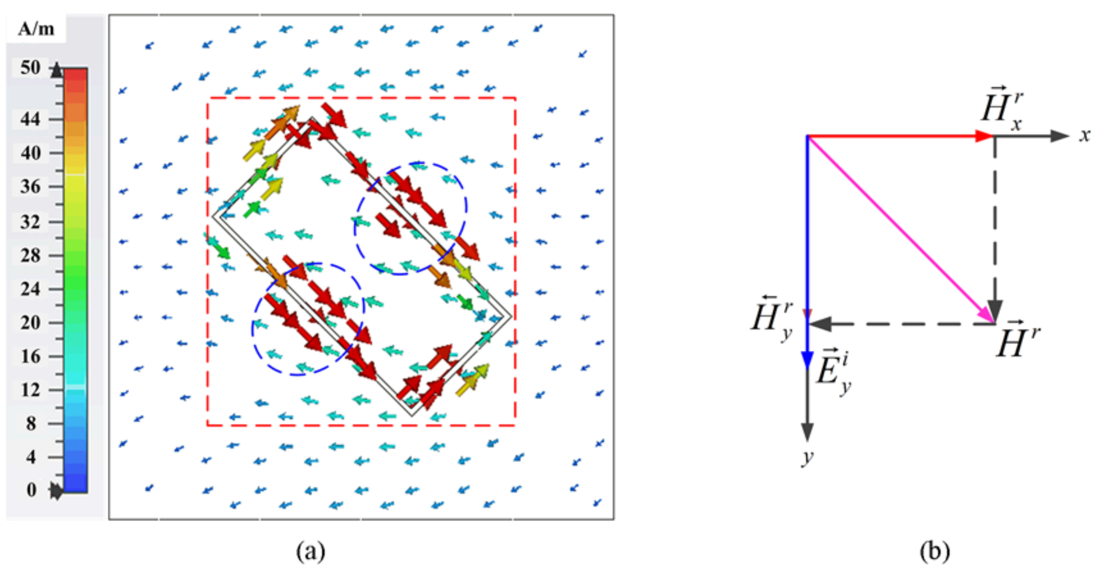

Figure 2. Induced current distribution of rectangular ring PCPS at 5.8 GHz and its decomposition diagram.

of the coupled E-field from the x-polarized TM_{10} mode to the y-polarized TM_{01} mode. Thus, mode cancellation was realized on the coupled antenna. Detailed parameters of the decoupling structure are as follows: $W_g = L_g = 41$ mm, $W = 10$ mm, $W_1 = 2.7$ mm, $L = 13$ mm, $L_1 = 6.5$ mm, $L_2 = 4$ mm, $d = 12$ mm, and $h = 1.6$ mm.

The aforementioned MIMO antenna is simulated and optimized using CST software to evaluate its radiation and isolation performance, with the simulated S-parameters displayed in Fig. 4. The reference antenna (without PCPS) demonstrated good matching, with the reflection coefficient surpassing 10 dB. In comparison, the isolation at 5.8 GHz was only approximately 12 dB. Upon introducing rectangular-ring PCPSs vertically between the antennas, the simulation results indicated that the PCPSs significantly contribute to suppressing mutual coupling in the MIMO antenna system. The highest isolation achieved was 49 dB at 5.8 GHz, while S_{11} was at −24 dB. Additionally, there was a slight reduction in the operating bandwidth of the antenna. This occurs because the decoupling structure closely resembles the reference antennas, and they all share the same substrate. EM radiation from the antenna can easily couple within the substrate, leading to a balance between the radiation performance and isolation performance of the antenna.

Decoupling mechanism

The operating mechanism of the decoupling effect due to the rectangular-ring PCPS can be presented by observing the surface current and E-field distributions of the proposed antenna at 5.8 GHz. In the following analysis, only Ant_1 was excited whereas Ant_2 was connected to a 50-Ω matched load.

Figure 5(a) shows the surface current distributions of the proposed antenna at 5.8 GHz, prior to the integration of rectangular-ring PCPSs. When Ant_1 was activated, it induced a coupling

https://doi.org/10.1017/S1759078724000461 Published online by Cambridge University Press

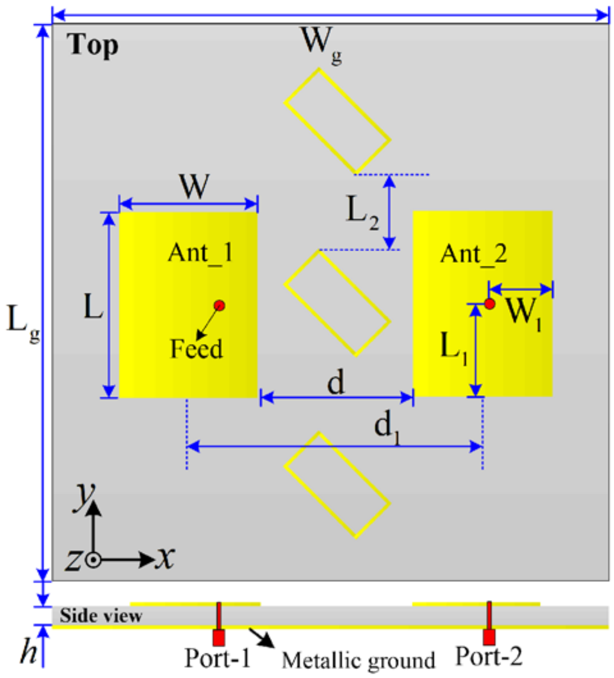

Figure 3. Structures of the proposed MIMO antenna.

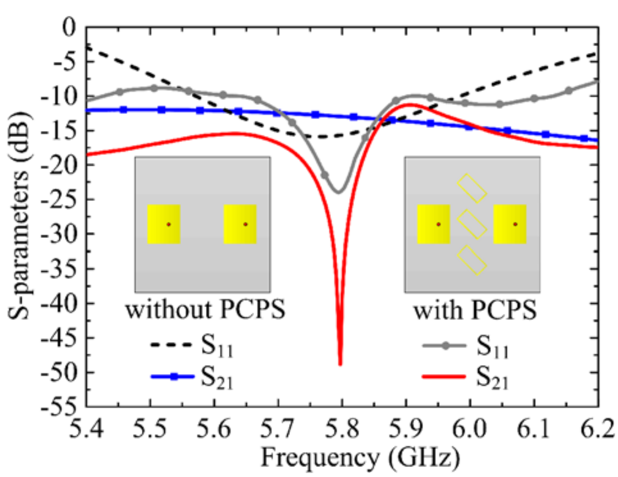

Figure 4. Simulated S-parameters of the proposed MIMO antenna.

current in Ant_2, moving in the same direction along the x-axis. Conversely, Fig. 5(b) shows that after adding PCPSs to the MIMO antenna, the coupling current Ant_2 adopts an orthogonal direction when compared to its initial distribution. This change shifts the reciprocating movement of the coupling current from the x-axis to the y-axis for Ant_2, significantly reducing the coupling current it receives. Furthermore, while various types of coupling, such as surface wave, near-field, and far-field coupling exist in MPA arrays, surface wave coupling is the predominant form when the substrate's electrical thickness meets certain criteria [33]:

$$\frac{h}{\lambda_0} \geqslant \frac{0.3}{2\pi\sqrt{\varepsilon_r}} \tag{2}$$

where h and ε_r denote the thickness and relative permittivity of the substrate, respectively; λ_0 denotes the wavelength in free space.

Figure 6 further illustrates the E-field distribution of the antenna at 5.8 GHz, reinforcing the effectiveness of the proposed decoupling structure. In Fig. 6(a), the reference MIMO antenna shows strong E-fields on the left and right sides, but these fields are considerably weaker in the center. This pattern indicates that Ant_1 is functioning in the TM_{10} mode. A similar E-field distribution is observed in the coupled, passive Ant_2. However, in Fig. 6(b), with the inclusion of the PCPS decoupling structure, the structure's capacity to transform the coupling E-field from x-polarization TM_{10} mode to y-polarization TM_{01} mode becomes apparent. Hence, Ant_2 receives simultaneous coupling from the TM_{10} mode of Ant_1 and TM_{01} mode of the decoupling structure. This coupling leads to the E-fields of the two modes in passive Ant_2 neutralizing each other, thereby creating an area of weak field. Consequently, when the feed position of passive Ant_2 is located in this weak-field area, it is less effectively excited due to reduced port energy, resulting in a significant decrease in mutual coupling to −49 dB.

Figures 6(c–g) depict the development of a weak-field region in MPA-2, a key aspect of the proposed self-decoupling method. Figure 6(e) illustrates that, when operating exclusively in the TM_{10} mode, the E-fields on the left and right sides of the patch antenna are in opposing directions. Similarly, Fig. 6(f) demonstrates that when functioning solely in the TM10 mode, the E-fields at the top and bottom of the patch are also opposite. In the designed MIMO antenna, both TM_{10} and TM_{01} modes are simultaneously coupled to Ant_2. Figure 6(g) shows that the intersection of these opposing fields leads to a significant weakening of the field intensity in certain areas, resulting in the formation of a weak-field region.

Fabrication and measured results

In this section, to verify the feasibility, a prototype of the proposed 1×2 MIMO MPA array is fabricated and measured. In the following subsections, analysis and discussions on the key parameters are presented.

S-parameters

A photograph of the prototype MIMO antenna, together with the simulated and measured S-parameter results, is shown in Fig. 7. As expected, the S-parameter simulation shown in Fig. 7(a) is consistent with the measured results, and the center frequency of the MIMO antenna approximately corresponds to 5.8 GHz. The operating bandwidth is $|S_{11}|$ <- 10 dB in the range of 5.65–5.9 GHz. Simultaneously, the isolation was greater than 15 dB in the operating bandwidth, and the maximum port isolation at the resonant frequency was 49 dB. Additionally, the frequency deviation was primarily due to the inaccurate dielectric constant of the substrate.

Radiation characteristic

Figure 8 illustrates the simulated and measured radiation patterns of the proposed MIMO antenna at 5.8 GHz in E/H-plane, both with and without the PCPS. The measured results align well with the simulated outcomes, indicating that the PCP decoupling structure does not significantly impact the antenna's radiation pattern. At 5.8 GHz, the realized gain of the MIMO antenna was observed to be 5.17 dBi. Additionally, the antenna's cross-polarization was significantly reduced following the decoupling process.

The simulated and measured boresight gains of the proposed 1×2 MIMO antenna array are illustrated in Fig. 9, showing

https://doi.org/10.1017/S1759078724000461 Published online by Cambridge University Press

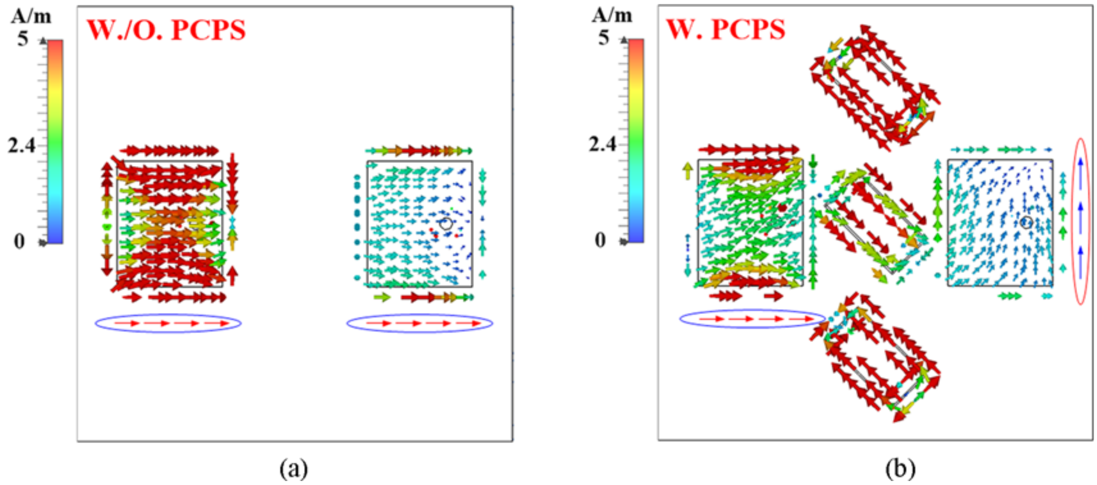

Figure 5. Simulated surface current distributions of the proposed MIMO antenna at 5.8 GHz. (a) Without and (b) with PCPS.

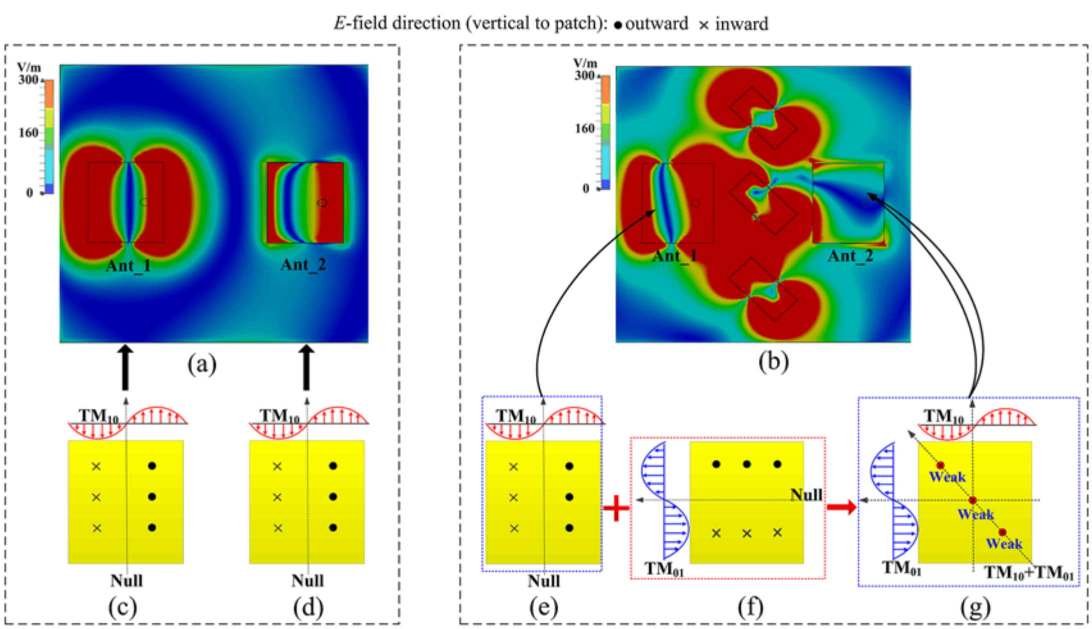

Figure 6. Simulated E-field distribution of the reference and proposed MIMO MPA array at 5.8 GHz. (a) Without PCPS. (b) With PCPS. (c) TM_{10} mode. (d) TM_{10} mode. (e) TM_{10} mode. (f) TM_{01} mode. (g) TM_{10} and TM_{10} modes.

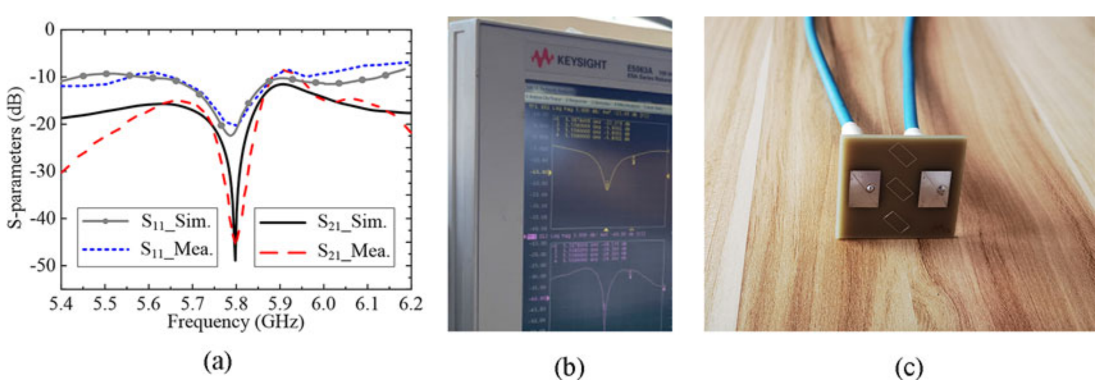

Figure 7. Simulated and measured results of the proposed MIMO MPA array. (a) S-parameters results, (b) S-parameter measurement photos, and (c) photos of the fabricated antenna.

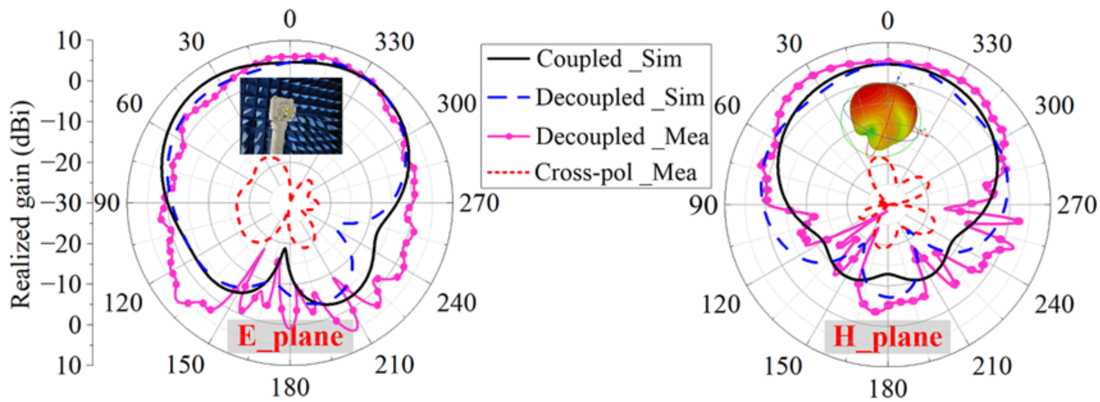

Figure 8. Radiation patterns of the proposed antenna at 5.8 GHz. (a) E-plane and (b) H-plane.

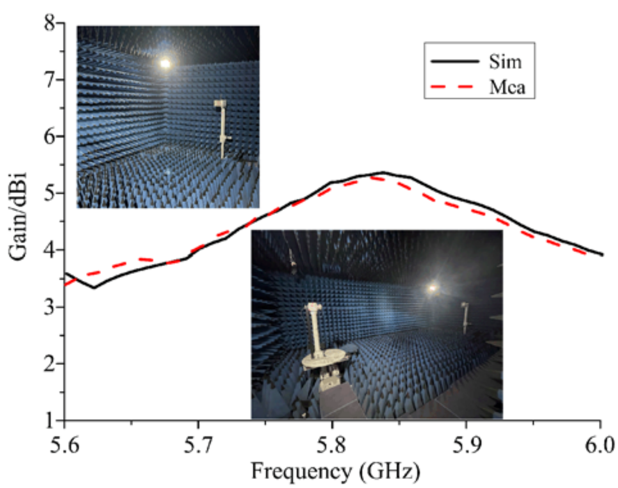

Figure 9. Simulated and measured boresight gains.

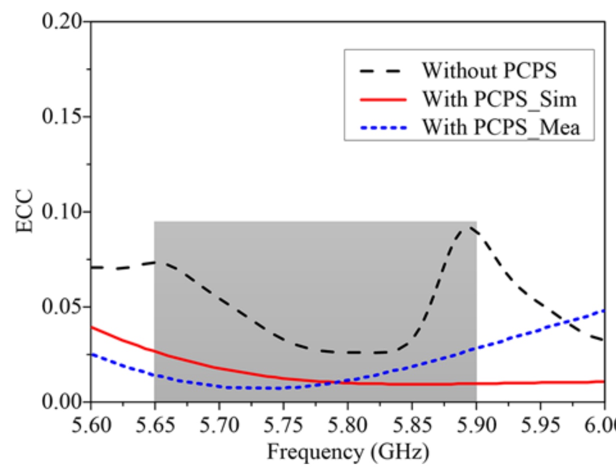

Figure 10. Simulated and measured ECC of the proposed MIMO antenna.

that their curves exhibit nearly the same trend in the operating frequency band. Within the operating frequency band of 5.65–5.9 GHz, the measured boresight gain varied between 3.81 and 5.31 dBi, and the maximum and average gain were 5.31 and 4.52 dBi, respectively.

MIMO-related performance

The envelope correlation coefficient (ECC) is an important index of an MIMO antenna, and it can be calculated using Equation (3) [34, 35] as follows:

$$ECC = \frac{\left| \int_0^{2\pi} \int_0^{\pi} \left(XPR \cdot E_{\theta i} \cdot E_{\theta j}^* \cdot P_\theta + E_{\phi i} \cdot E_{\phi j}^* \cdot P_\varphi \right) d\Omega \right|^2}{\int_0^{2\pi} \int_0^{\pi} \left(XPR \cdot E_{\theta i} \cdot E_{\theta i}^* \cdot P_\theta + E_{\phi i} \cdot E_{\phi i}^* \cdot P_\phi \right) d\Omega \times \int_0^{2\pi} \int_0^{\pi} \left(XPR \cdot E_{\theta j} \cdot E_{\theta j}^* \cdot P_\theta + E_{\phi j} \cdot E_{\phi j}^* \cdot P_\phi \right) d\Omega}. \tag{3}$$

$$XPR(dB) = 10 \cdot \log_{10} \frac{P_V}{P_H} \tag{4}$$

where i and j denote the numbers of ports, XPR denotes the cross-polarization ratio, E denotes the incident electric field, and P_θ and P_ϕ denote the θ and φ components of the angular density functions of the incoming wave, respectively, and Ω denotes the solid angle of the spherical coordinate.

Within the impedance bandwidth of 5.65–5.9 GHz, the ECC of the proposed MIMO antenna was less than 0.025 after loading PCPS, which was much lower than that of the original MIMO antenna (Fig. 10).

Comparison

Table 1 provides a comparative analysis of the decoupling approaches proposed in this study with those previously reported. Previous studies [17–19] have documented structures capable of generating polarized rotational effects for decoupling purposes. The PCP isolator design in paper [17] was noted for its complexity, requiring multiple optimizations in its connection form. Additionally, the MPA array in paper [17] necessitated the inclusion of circular slots to mitigate the cross-polarized field. Similarly, the implementation of L-shaped stubs was essential in the MPA array of paper [19] for reducing the cross-polarized field. In paper [18], the spacing between array elements in an MIMO antenna was approximately 0.53λ_0 greater than half the wavelength. Conversely, this study introduces a rectangular-ring polarization–rotation decoupling structure that is not only simpler but also demonstrates a clear decoupling effect without compromising the antenna's performance.

Table 1. Comparison of performance with previously reported antennas

Ref./Year	Decoupling method	Antenna size (λ_0^2) (mm^2)	Operating bandwidth (GHz)	Resonant frequency (GHz)	Center-to-center spacing	Isolation enhancement	Design complexity	Additional structure
[9]/2020	DGS	1.01 × 0.51 (240 × 120)	1.258–1.278 (20 MHz)	1.268	$0.50\lambda_0$	16→47 dB	High	No
[12]/2019	Metasurface	1.15 × 0.81 (99 × 70)	3.52–3.57 (50 MHz)	3.5	$0.40\lambda_0$	8.4→50 dB	High	No
[17]/2017	Polarization-conversion isolator	NG	5.68–5.9 (220 MHz)	5.8	$0.39\lambda_0$	12.5→34.8 dB	High	Yes
[18]/2017	Polarization transformation DGS	NG	2.245–2.3 (55 MHz)	2.27	$0.53\lambda_0$	15→30 dB	High	Yes
[19]/2023	U-Shaped polarization converter	1.17 × 0.83 (70 × 50)	4.93–5.15 (220 MHz)	5	$0.325\lambda_0$	20→34 dB	High	Yes
[22]/2020	Weak-field-based	1.2 × 0.7 (105 × 60)	3.43–3.56 (130 MHz)	5.8	$0.50\lambda_0$	24→61 dB	Low	No
[24]/2023	Higher-order modes	NG	5.0–5.5 (500 MHz)	5.25	$0.50\lambda_0$	15→45 dB	High	Yes
This work	PCPS	0.47 × 0.47 (41 × 41)	5.65–5.9 (250 MHz)	5.8	$0.42\lambda_0$	12→49 dB	Low	No

Notes: λ_0: free-space wavelength at the center frequency. 16→47 indicates that the isolation between the antennas is improved from 16 to 47 dB. NG = not given.

In the case of previous studies [9, 12, 22, 24], although the MIMO arrays realized self-decoupling without using any additional decoupling structure [22, 24], the method primarily relied on the characteristics of the radiator. Additionally, several defects were observed in these designs. For example, the self-decoupled MPA array reported in paper [22] is limited to the specific inset feed scheme. In contrast, the DRA array reported in paper [24] employs the higher-order mode of DRA, which considerably increases the height (volume) of antenna elements. Meanwhile, the self-decoupling MIMO antenna exhibits the disadvantage of large array element spacing. A metasurface structure is typically placed above the antenna or inserted in the middle of the antenna elements in the loading method. Given that the distance between the metasurface structure and the antenna element significantly affects the isolation performance, the profile height of the antenna increases substantially [12].

Conclusions

In this study, a systematic approach is proposed to enhance the isolation between coupled MPA using a rectangular-ring PCP decoupling structure. First, the unit cell of the rectangular-ring PCPS was designed and analyzed independently, and its operating bandwidth was adjusted to match the operating frequency of the reference MIMO antenna. The simulation results demonstrated that the rectangular-ring PCPS efficiently converts the x-polarized E-field into orthogonal y-polarization. Based on this characteristic, a rectangular-ring PCPS was loaded onto a two-element MIMO MPA. Furthermore, TM_{10} mode from the excited antenna (Ant_1) and TM_{01} mode from the decoupling structure were concurrently coupled to the passive antenna (Ant_2), forming an evident weak-field region on the passive Ant_2. Therefore, when the feeding position of passive Ant_2 was located in the weak-field region, Ant_2 could not be effectively excited. Hence, extremely low mutual coupling was obtained. Furthermore, the decoupling principle was described in detail based on the distributions of the E-field and surface current before and after antenna decoupling. Finally, the antenna's performance was measured and compared with those reported in the literature. The comparison shows that the decoupling structure proposed in this study exhibits the advantages of a simple structure, low profile, and no requirements to introduce additional structures to improve the cross-polarization of the antenna. Notably, the concept of polarization conversion is often applied to methods such as radar cross-section reduction and circularly polarized antenna design. This study systematically applied it to the suppression of MIMO antenna array coupling, and thereby, further expanding its application range.

Acknowledgements. This study was supported in part by the Doctoral Innovation Fund of the Xi'an University of Technology under Grant 310-252072219 and in part by the National Natural Science Foundation of China under Grant 62101440.

Competing interests. The authors report no conflict of interest.

References

1. **Xu H, Liang Z and Li Y** (2022) A high-gain microstrip magnetic dipole antenna utilizing slot-loaded high-order mode for WLAN applications. *IEEE Transactions on Antennas and Propagation* **70**, 9130–9138.
2. **Guo C, Li J and Yang D** (2022) Compact co-polarized decoupled microstrip patch array antenna based on TM_{02}/TM_{03} modes cancellation. *IEEE Transactions on Antennas and Propagation* **70**, 9906–9911.
3. **Ren A, Liu Y and Sim C** (2019) A compact building block with two shared-aperture antennas for eight-antenna MIMO array in metal-rimmed smartphone. *IEEE Transactions on Antennas and Propagation* **67**, 6430–6438.
4. **Kumar A and Imaculate Rosaline S** (2021) Hybrid half-mode SIW cavity-backed diplex antenna for on-body transceiver applications. *Applied Physics A* **127**, 1–7.
5. **Kumar A, Chaturvedi D and Raghavan S** (2019) Dual-band, dual-fed self-diplexing antenna. In *2019 13th European Conference on Antennas and Propagation (EuCAP)*, 1–5.

6. **Ren A, Yu H and Yang L** (2023) A broadband MIMO antenna based on multimodes for 5G smartphone applications. *IEEE Antennas and Wireless Propagation Letters* **22**, 1642–1646.
7. **Zhang W, Li Y and Wei K** (2023) A dual-band MIMO antenna system for 2.4/5 GHz WLAN applications. *IEEE Transactions on Antennas and Propagation* **71**, 5749–5758.
8. **Wong K, Chen J and Li W** (2021) Integrated four low-profile shorted patch dual-band WLAN MIMO antennas for mobile device applications. *IEEE Transactions on Antennas and Propagation* **69**, 3566–3571.
9. **Gao D, Cao Z and Fu S** (2020) A novel slot-array defected ground structure for decoupling microstrip antenna array. *IEEE Transactions on Antennas and Propagation* **68**, 7027–7038.
10. **Qian B, Chen X and Kishk A** (2021) Decoupling of microstrip antennas with defected ground structure using the common/differential mode theory. *IEEE Antennas and Wireless Propagation Letters* **20**, 828–832.
11. **Tan X, Wang W and Wu Y** (2019) Enhancing isolation in dual-band meander-line multiple antenna by employing split EBG structure. *IEEE Transactions on Antennas and Propagation* **67**, 2769–2774.
12. **Luan H, Chen C and Chen W** (2019) Mutual coupling reduction of closely E/H-plane coupled antennas through metasurfaces. *IEEE Antennas and Wireless Propagation Letters* **18**, 1996–2000.
13. **Jafargholi A, Jafargholi A and Choi J** (2018) Mutual coupling reduction in an array of patch antennas using CLL metamaterial superstrate for MIMO applications. *IEEE Transactions on Antennas and Propagation* **67**, 179–189.
14. **Liu R, An H and Zheng H** (2020) Neutralization line decoupling tri-band multiple-input multiple-output antenna design. *IEEE Access* **8**, 27081–27026.
15. **Li M, Wang M and Jiang L** (2021) Decoupling of antennas with adjacent frequency bands using cascaded decoupling network. *IEEE Transactions on Antennas and Propagation* **69**, 1173–1178.
16. **Li M, Zhang D and Wu K** (2022) Decoupling and matching network for dual-band MIMO antennas. *IEEE Transactions on Antennas and Propagation* **70**, 1764–1775.
17. **Cheng Y, Ding X and Shao W** (2017) Reduction of mutual coupling between patch antennas using a polarization-conversion isolator. *IEEE Antennas and Wireless Propagation Letters* **16**, 1257–1260.
18. **Wei K, Li J and Wang L** (2017) Microstrip antenna array mutual coupling suppression using coupled polarisation transformer. *IET Microwaves, Antennas & Propagation* **11**, 1836–1840.
19. **Odabasi H, Salimitorkamani M and Turan G** (2023) Mutual coupling reduction between closely placed patch antennas using complementary U-shaped polarization converter. *IEEE Antennas and Wireless Propagation Letters* **22**(11), 2710–2714.
20. **Song W, Zhu X and Wang L** (2022) Simple structure E-plane decoupled millimeter wave antenna based on current cancellation model. *IEEE Transactions on Antennas and Propagation* **70**, 9871–9876.
21. **Abbasi M, Aziz A and Malik W** (2022) A simple and modular MIMO antenna system for closely spaced patch antennas. *Microwave and Optical Technology Letters* **64**, 1210–1216.
22. **Lin H, Chen Q and Ji Y** (2020) Weak-field-based self-decoupling patch antennas. *IEEE Transactions on Antennas and Propagation* **68**, 4208–4217.
23. **Lai Q, Pan Y and Zheng S** (2021) Mutual coupling reduction in MIMO microstrip patch array using TM_{10} and TM_{02} modes. *IEEE Transactions on Antennas and Propagation* **69**, 7562–7571.
24. **Pan Y, Hu Y and Zheng S** (2021) Design of low mutual coupling dielectric resonator antennas without using extra decoupling element. *IEEE Transactions on Antennas and Propagation* **69**, 7377–7385.
25. **Lai Q, Pan Y and Zheng S** (2023) A self-decoupling method for MIMO antenna array using characteristic mode of ground plane. *IEEE Transactions on Antennas and Propagation* **71**, 2126–2135.
26. **Tran H, Hussain N and Park H** (2022) Isolation in dual-sense CP MIMO antennas and role of decoupling structures. *IEEE Antennas and Wireless Propagation Letters* **21**, 1203–1207.
27. **Yuan X, Chen Z and Gu T** (2021) A wideband PIFA-pair-based MIMO antenna for 5G smartphones. *IEEE Antennas and Wireless Propagation Letters* **20**, 371–375.
28. **Tian X and Du Z** (2023) Wideband shared-radiator four-element MIMO antenna module for 5G mobile terminals. *IEEE Transactions on Antennas and Propagation* **71**, 4799–4811.
29. **Chang L and Liu H** (2022) Low-profile and miniaturized dual-band microstrip patch antenna for 5G mobile terminals. *IEEE Transactions on Antennas and Propagation* **70**, 2328–2333.
30. **Liu Z, Zhu L and Zhang X** (2019) A low-profile and high-gain CP patch antenna with improved AR bandwidth via perturbed ring resonator. *IEEE Antennas and Wireless Propagation Letters* **18**, 397–401.
31. **Qiu Y, Weng Z and Hou D** (2023) Bandwidth enhancement of metasurface antennas by shifting and reshaping high-order mode. *IEEE Antennas and Wireless Propagation Letters* **22**, 933–937.
32. **Zheng Q, Guo C and Ding J** (2018) Wideband metasurface-based reflective polarization converter for linear-to-linear and linear-to-circular polarization conversion. *IEEE Antennas and Wireless Propagation Letters* **17**, 1459–1463.
33. **Nikolic M, Djordjevic A and Nehorai A** (2005) Microstrip antennas with suppressed radiation in horizontal directions and reduced coupling. *IEEE Transactions on Antennas and Propagation* **53**, 3469–3476.
34. **Karaboikis M, Papamichael V and Tsachtsiris G** (2008) Integrating compact printed antennas onto small diversity/MIMO terminals. *IEEE Transactions on Antennas and Propagation* **56**, 2067–2078.
35. **Khan M, Capobianco A and Najam A** (2014) Compact ultra-wideband diversity antenna with a floating parasitic digitated decoupling structure. *IET Microwaves, Antennas & Propagation* **8**, 747–753.

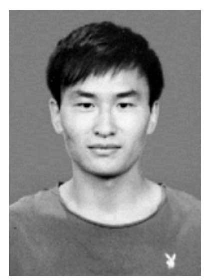

Zhonghong Du was born in Tianshui, Gansu, China, in 1994. He received the B.S. in Electronic Information from Xi'an University of Technology, Xi'an, China, in 2017, and M.S. in Communicating Engineering from Xi'an University of Technology, Xi'an, China, in 2020. Where he is currently pursuing the Ph.D. degree in Electromagnetic Field and Microwave Technology. His research interests include MIMO antennas decoupling technology, electromagnetic metasurface, and RF circuits. He serves as a reviewer for the IEEE Antennas and Wireless Propagation Letters, International Journal of Microwave and Wireless Technologies.

Xiaohui Zhang received his B.S. in Industrial Automation in 1995, his M.S. in Control Science and Engineering in 2002, his Ph.D. degree in Control Science and Engineering in 2009, all from Xi'an University of Technology in Xi'an, China. He is currently a professor of Information and Control Department at Xi'an University of Technology, Xi'an, China. His recent research interests include advanced navigation, signal processing and pattern recognition, electromagnetic technology, and antenna design.

Peiyu Qin received her B.S. in Information Engineering from Tianjin Normal University, Tianjin, China, in 2019. She is currently a graduate student at Xi'an University of Technology, Xi'an, China. Currently, she is engaged in research on MIMO antenna coupling suppression and polarization rotation isolation structure at the Department of Electronic and Electrical Engineering, Brunel University, London, United Kingdom.

https://doi.org/10.1017/S1759078724000461 Published online by Cambridge University Press

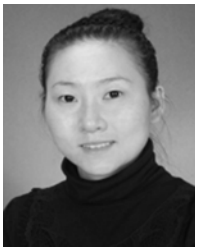

Yurong Pu received the B.S., M.S., and Ph.D. degrees in Electronic Engineering from the Xi'an University of Technology (XUT), Xi'an, China, in 2004, 2007, and 2013, respectively. She is currently an associate professor with the Department of Electronic Engineering, XUT. Her current research interests include computational electromagnetics and wave propagation.

Xiaoli Xi received her B.S. in Applied Physics from the University of Defense Technology in Changsha, China, in 1990, her M.S. in Biomedical Engineering from the Fourth Military Medical University in Xi'an, China, in 1998, and her Ph.D. degree in Electrical Engineering from the Xi'an Jiaotong University in Xi'an, China, in 2004. She is currently a Professor with the Electronics Engineering Department, Xi'an University of Technology, Xi'an, China. Her current research interests include wave propagation, antenna design, and communication signals processing. She serves as a reviewer for the IEEE Transactions on Microwave Theory and Techniques, IEEE Transactions on Antennas and Propagation, International Journal of Microwave and Wireless Technologies, IET Microwaves Antennas & Propagation, IEEE Access, and IEEE Antennas and Wireless Propagation Letters.

https://doi.org/10.1017/S1759078724000461 Published online by Cambridge University Press